

73 FILE 0007
GL-TR-89-0106

The Sensitivity of Middle East Precipitation
and Cloud Forecasts to Changes in Eastern
Mediterranean Sea Surface Temperatures

AD-A207 864

Stephen Brenner

Israel Oceanographic and
Limnological Research Ltd
National Institute of Oceanography
P.O. Box 8030
Haifa 31080, ISRAEL

1 March 1989

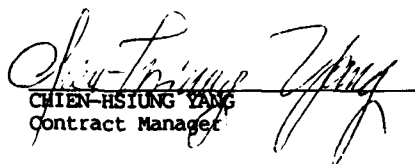
FINAL REPORT
1 October 1986-31 December 1988

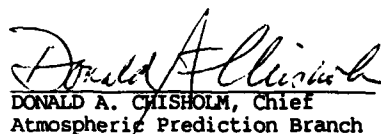
APPROVED FOR PUBLIC RELEASE; DISTRIBUTION UNLIMITED

GEOPHYSICS LABORATORY
AIR FORCE SYSTEMS COMMAND
UNITED STATES AIR FORCE
HANSOM AIR FORCE BASE, MASSACHUSETTS 01731-5000

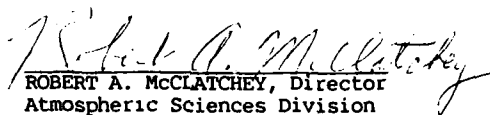
44
A

This technical report has been reviewed and is approved for publication.


CHIEN-HSIUNG YANG
Contract Manager


DONALD A. CHISHOLM, Chief
Atmospheric Prediction Branch

FOR THE COMMANDER


ROBERT A. McCLATCHEY, Director
Atmospheric Sciences Division

This report has been reviewed by the ESD Public Affairs Office (PA) and is releasable to the National Technical Information Service (NTIS).

Qualified requestors may obtain additional copies from the Defense Technical Information Center. All others should apply to the National Technical Information Service.

If your address has changed, or if you wish to be removed from the mailing list, or if the addressee is no longer employed by your organization, please notify GL/DAA, Hanscom AFB, MA 01731. This will assist us in maintaining a current mailing list.

Do not return copies of this report unless contractual obligations or notices on a specific document require that it be returned.

Unclassified
SECURITY CLASSIFICATION OF THIS PAGE

REPORT DOCUMENTATION PAGE				
1a. REPORT SECURITY CLASSIFICATION Unclassified		1b. RESTRICTIVE MARKINGS		
2a. SECURITY CLASSIFICATION AUTHORITY		3. DISTRIBUTION / AVAILABILITY OF REPORT Approved for public release; distribution unlimited		
2b. DECLASSIFICATION / DOWNGRADING SCHEDULE				
4. PERFORMING ORGANIZATION REPORT NUMBER(S)		5. MONITORING ORGANIZATION REPORT NUMBER(S) GL-TR-89-0106		
6a. NAME OF PERFORMING ORGANIZATION Israel Oceanographic and Limnological Research Ltd.	6b. OFFICE SYMBOL (If applicable)	7a. NAME OF MONITORING ORGANIZATION Geophysics Laboratory		
6c. ADDRESS (City, State, and ZIP Code) P.O. Box 8030 Tel Shikmona Haifa 31080 ISRAEL		7b. ADDRESS (City, State, and ZIP Code) Hanscom AFB Massachusetts 01731-5000		
8a. NAME OF FUNDING / SPONSORING ORGANIZATION EOARD	8b. OFFICE SYMBOL (If applicable) LGS	9. PROCUREMENT INSTRUMENT IDENTIFICATION NUMBER AFOSR-87-0066		
8c. ADDRESS (City, State, and ZIP Code) 223/231 Old Marylebone Rd. London NW1 5TH ENGLAND		10. SOURCE OF FUNDING NUMBERS		
		PROGRAM ELEMENT NO. 61102F	PROJECT NO. 2301	TASK NO. D1
11. TITLE (Include Security Classification) The Sensitivity of Middle East Precipitation and Cloud Forecasts to Changes in Eastern Mediterranean Sea Surface Temperatures.				
12. PERSONAL AUTHOR(S) Brenner, Stephen				
13a. TYPE OF REPORT Final	13b. TIME COVERED FROM 1 Oct 86 TO 31 Dec 88	14. DATE OF REPORT (Year, Month, Day) 1 March 1989	15. PAGE COUNT 38	
16. SUPPLEMENTARY NOTATION				
17. COSATI CODES			18. SUBJECT TERMS (Continue on reverse if necessary and identify by block number)	
FIELD	GROUP	SUB-GROUP	Mediterranean weather systems; precipitation forecasts; numerical weather prediction; global models.	
19. ABSTRACT (Continue on reverse if necessary and identify by block number)				
<p>Air sea interaction over the eastern Mediterranean plays an important role in shaping the weather of the Middle East. In this region, the year can be divided into two main seasons, a hot dry summer from April to September and a cool wet winter from October to March. precipitation in this region is usually associated with migratory cyclones which cross the Mediterranean and bring cold air masses from Europe.</p> <p>Several recent statistical studies of this region have shown that there is a very high correlation between the sensible and latent heat fluxes from the eastern Mediterranean and the corresponding seasonal precipitation over this region. While these studies clearly demonstrate the importance of the sea, they do not explain the physical processes involved.</p> <p>To further understand this relationship, we have run a series of numerical experiments</p> <p style="text-align: right;">(continued)</p>				
20. DISTRIBUTION / AVAILABILITY OF ABSTRACT <input checked="" type="checkbox"/> UNCLASSIFIED/UNLIMITED <input type="checkbox"/> SAME AS RPT. <input type="checkbox"/> DTIC USERS			21. ABSTRACT SECURITY CLASSIFICATION Unclassified	
22a. NAME OF RESPONSIBLE INDIVIDUAL Chien-Hsiung Yang			22b. TELEPHONE (Include Area Code)	22c. OFFICE SYMBOL GL/LYP

DD FORM 1473, 84 MAR

83 APR edition may be used until exhausted.
All other editions are obsolete.

SECURITY CLASSIFICATION OF THIS PAGE
Unclassified

Block 19. continued

with a global model which is based on the AFGL baseline model. A set of eleven 96 hour forecast were run. In each case two experiments were conducted, one in which the sea surface temperatures were fixed at their climatological monthly mean values and one in which the temperature of the eastern Mediterranean was increased by up to 2.5 degrees. In the control runs, it was found that the rainfall in this region was produced primarily by the convective scheme of the model. In the anomaly runs, the rainfall increased mainly over the area of the imposed anomaly and over the surrounding region. The increase in rainfall was traced to the combined effects of additional moisture availability due to enhanced evaporation and increased convective activity due to the destabilizing effect of heating from below by the enhanced sensible heat flux.

A detailed study was made of the 6 November 1986 case in which we ran several experiments with different anomaly magnitudes and with different model resolutions. The overall agreement between the low and high resolution runs is very encouraging. There are of course differences in the details due to the ability of the higher resolution model to better represent smaller scale features in the humidity field.



A-1

5 072

Table of Contents

Publications	iv
Acknowledgements	v
1. INTRODUCTION	1
2. MODIFICATION TO THE AFGL BASELINE MODEL	2
2.1 Surface fixed fields	2
2.2 Planetary boundary layer scheme	4
2.3 Moist convective scheme	7
2.4 Diagnostic cloud scheme	8
3. EXPERIMENTS AND RESULTS	9
3.1 Data sources	9
3.2 Low resolution experiments	10
3.3 Case study - 6 November 1986	21
4. CONCLUSIONS	29
5. REFERENCES	32

Publications

The following publications and reports have been prepared under this grant:

1. Brenner, S., 1987: Derivation of consistent surface fixed fields for use in a global NWP model. AFOSR Sci. Rep. 87-0066-001, 19pp.
2. Brenner, S. 1988: Sensitivity of Middle East precipitation forecasts to eastern Mediterranean sea surface temperature anomalies (Abstract). Reprints of the Seventh Conference on Ocean-Atmosphere Interaction, 1-5 February 1988, Anaheim, CA. American Meteorological Society, 101.
3. Brenner, S., 1988: A comparison of various numerical solutions of the hydrostatic equation. Reprints of the Eighth Conference on Numerical Weather Prediction, 22-26 February 1988, Baltimore, MD. American Meteorological Society, 438-441.
4. Brenner, S., 1989: The influence of eastern Mediterranean sea surface temperatures on regional precipitation. To be submitted.

Acknowledgements

We wish to acknowledge the European Center for Medium Range Weather Forecasts (ECMWF) for providing the data used to run the experiments described in this report. Mr. A. Kovarsky of our computer department was helpful in preparing the programs to read the data tapes. Thanks go to Mr. Z. Rosentroub of the physical oceanography department for many helpful and insightful discussions on the relationship between eastern Mediterranean sea surface temperatures and rainfall in Israel. And finally, many thanks to Ms. H. Bernard for expertly preparing the figures and helping to arrange the layout of this report.

1. INTRODUCTION

Air sea interaction over the eastern Mediterranean plays an important role in shaping the weather of the Middle East. In this region, the year can be divided into two main seasons, a hot dry summer from April to September and a cool wet winter from October to March. Precipitation in this area is usually associated with migratory cyclones which cross the Mediterranean and bring cold air masses from Europe (Tzvetkov et al., 1985). On occasion, a secondary low will form over the sea in the vicinity of Cyprus. These so called Cyprus lows will often enhance the precipitation in this region. Ozsoy (1981) noted that cyclogenetic activity in this region is also associated with strong interaction between the Subtropical and the Polar Front jet streams.

The seasonal rainfall over the eastern Mediterranean is heaviest along the northern and eastern coasts and generally decreases southward and eastward. In a statistical study of the region, Tzvetkov and Assaf (1982) found a remarkably high correlation of 0.9 between winter precipitation in Israel and what they termed heat storage extraction from the eastern Mediterranean. While these results clearly demonstrate the importance of the sea they do not explain the physical mechanism responsible.

In this report, we have taken the first step in understanding the complex physical processes that control rainfall in this region. In order to accomplish this, we have used a modified version of the global model developed at the Air Force Geophysics Laboratory (AFGL). In Section 2 we describe the changes that were implemented in the model while in Section 3 we present results from a series of experiments in which the sea surface temperatures in the eastern Mediterranean were varied from their climatological mean values. Section 4 contains our conclusions.

2. MODIFICATIONS TO THE AFGL BASELINE MODEL

The AFGL baseline model has already been described in detail by Brenner et al. (1982, 1984) and will only be briefly summarized here. It is a global primitive equation model on a longitude, latitude, sigma grid. The horizontal representation is handled spectrally while the vertical differencing is based on the quadratic conserving scheme described by Arakawa and Lamb (1977). The time scheme is semi-implicit. Subgrid scale physical parameterizations are based on the schemes used in the previous version of the National Meteorological Center (NMC) global spectral model (Sela, 1980). These include: (i) bulk aerodynamic formulae for surface drag, sensible heat flux, and evaporation (the latter two over the oceans only); (ii) Kuo (1965) type moist convection; (iii) large scale condensation; (iv) dry convective adjustment; and (v) horizontal diffusion. In this section we will describe the modifications that we made to the baseline model for the purposes of our study. Our efforts focused mainly on improving the planetary boundary layer scheme of the model.

2.1 Surface fixed fields

The surface fixed fields in a numerical model describe the physical structure of the surface of the earth. These form an integral part of any scheme designed to simulate the interaction between the atmosphere and the solid earth. For the AFGL baseline model, these fields include topography, land sea mask, sea surface temperature, and the neutral drag coefficient. A procedure for deriving consistent surface fixed fields for this model has been described by Brenner (1987) and will only be briefly

reviewed here. The method is based on the assumption that the basic data is available on a $2.5^{\circ} \times 2.5^{\circ}$ latitude longitude grid. The required values for the model are derived from this basic data set by interpolating onto the model grid with a procedure that is similar to one pass of a Cressman (1959) type of objective analysis.

The AFGL baseline model, as many other models, uses a smoothed topography which is generated by subjecting the $2.5^{\circ} \times 2.5^{\circ}$ data to various smoothing operators and then interpolating onto the model grid. Recently it has been recognized that using a rougher topography could be beneficial in improving medium range forecasts. The attempt to incorporate the effects of the subgrid scale variance of the topography has resulted in various concepts such as envelope orography (Wallace et al., 1983) and step mountains (Mesinger, 1985). However, the "best" representation of topography, especially in spectral models, has not yet been established. For our study we have adopted an approach which is somewhere between the smoothed topography and the various rough topographies mentioned above. We begin with the $1^{\circ} \times 1^{\circ}$ topography supplied by NCAR. These data are first interpolated onto the $2.5^{\circ} \times 2.5^{\circ}$ grid on which the other surface fields are available. The $2.5^{\circ} \times 2.5^{\circ}$ values are then interpolated onto the model grid according to the method of Brenner (1987). The most noticeable differences are the higher elevations over South America and around the Mediterranean basin and the steeper slopes in the Himalayas.

The land sea mask is a flag which tells the model if the surface is land or sea for the purposes of surface flux calculations in the planetary boundary layer scheme. In the AFGL baseline model, the land sea mask is based on the sea surface temperature field so that any given grid point can be either all land or all sea. For this study a land sea mask was derived which allows for partial

land coverage in a grid box. The $2.5^\circ \times 2.5^\circ$ values were derived in conjunction with the topography field based on the original $1^\circ \times 1^\circ$ topography data. The required values on the model grid are obtained via the same interpolation/analysis method used for topography. The land sea mask and the topography on the model grid are consistent in the sense that any grid point defined as all sea cannot have an elevation different from zero before the spectral decomposition of the topography field.

The sea surface temperatures used in this study are the climatological monthly mean values which are available on the $2.5^\circ \times 2.5^\circ$ grid. They are interpolated onto the model grid using the same method as for topography and the land sea mask. The temperature of sea ice is set to 271.15 K. Surface temperature over land is a time dependent field which is obtained by extrapolating downward according to the lapse rate in the two lowest model layers (Bourke, et al., 1977).

Finally, the basic values for the neutral drag coefficients are geographically varying (depending upon the roughness length) and are available on the $2.5^\circ \times 2.5^\circ$ grid. These are also interpolated onto the model grid in the manner outlined above.

2.2 Planetary boundary layer scheme

As mentioned above, the planetary boundary layer (PBL) scheme in the AFGL baseline model consists of bulk formulae for surface drag, sensible heat flux, and evaporation, the latter two being allowed only over the oceans. The drag coefficient is set to its neutral value while the coefficients for sensible and latent heat fluxes include an additional factor to account for wind speed dependence. Other than the surface fluxes into the lowest layer

of the model, there is no vertical diffusion allowed. Since our major interest in this research is air sea interaction, we felt it necessary to improve upon the baseline PBL scheme. However, due to computer resource limitations, we were not able to adapt an overly complex scheme such as the one developed by Mahrt et al. (1984) for AFGL. Instead we settled on the scheme described below which we feel is a reasonable compromise between being state of the art yet computationally efficient.

Vertical diffusion is incorporated in the model following the linearized formulation of Bourke et al. (1977). A term of the form

$$\frac{g}{p_s} \frac{\partial F}{\partial \sigma}$$

where g is gravity, p_s is the surface pressure, and $F = (\tau, H, E)$ is added to the momentum, thermodynamic, and moisture equations, respectively. For all levels except the surface, these fluxes are given by

$$\tau = \rho K_v \frac{\partial V}{\partial \sigma} \quad (1)$$

$$H = \rho K_v \frac{\partial \theta}{\partial \sigma} \quad (2)$$

$$E = \rho K_v \frac{\partial Q}{\partial \sigma} \quad (3)$$

where V is the horizontal wind vector, θ is the potential temperature, Q is the specific humidity, and the diffusion coefficient, K_v , is given by

$$K_v = \mu^2 \left| \frac{\partial V}{\partial z} \right| \quad (4).$$

The mixing length, μ , decreases linearly from the surface up to $\sigma = 0.5$ according to $60(\sigma - 0.5)$ m and is set to zero above $\sigma = 0.5$.

The surface fluxes are given by bulk formulae with stability dependent coefficients. The respective expressions are

$$\tau = -\rho C_M V_* V_* \quad (5)$$

$$H = \rho C_H V_* (Q_* - Q_K) \quad (6)$$

$$E = \rho C_E V_* (\theta_* - \theta_K) \quad (7)$$

where C_M , C_H , C_E are the bulk coefficients, V is the magnitude of the wind speed in the lowest model layer, and the subscripts * and K indicate values at the surface and at the lowest model layer respectively. The coefficients are functions of the bulk Richardson number, Ri , of the lowest half layer which is defined by

$$Ri = \frac{g h (\theta_K - \theta_*)}{\theta_K V_K^2} \quad (8)$$

where h is the height of the lowest layer. In determining the value of h it was found that the Arakawa vertical differencing scheme produces rather large errors due to the use of an integral constraint (Brenner, 1988). For this reason, h in the PBL scheme is computed according to the discrete hydrostatic equation described by Gordon and Stern (1982). For unstable stratification ($Ri < 0$), the bulk coefficients are given by

$$C_M = C_{D_W} \left[1 + \frac{7}{a} \ln(1 - a Ri) \right] \quad (9)$$

$$C_H = C_E = 1.5 C_M \quad (10)$$

Eqs. (9) is taken from Deardorff (1968) and the empirical constant, a , is given by $a = 0.83 C_{D_W}^{-0.42}$. Over land,

the neutral drag coefficient, C_{DN} , is taken from the fixed field values supplied on the $2.5^\circ \times 2.5^\circ$ grid interpolated on to the model grid. Over water, the values are given as a function of the surface wind speed

$$C_{DN} = [0.43 + 0.097 V] \times 10^{-3} \quad (11)$$

as in Geernaert et al. (1986).

For stable stratification ($Ri \geq 0$), the bulk coefficients are given by

$$C_H = C_{DN} \exp(-Ri) \quad (12)$$

$$C_H = C_E = \frac{1.35 C_H}{1 + 1.93 Ri} \quad (13).$$

Eq. (12) is taken from Mahrt (1987) and eq. (13) is from Hansen et al. (1983).

Finally, the surface wind is taken as the wind of the lowest model layer rotated towards lower pressure. The turning angle, α , depends upon the stability and type of surface. Over land the values are 30° for $Ri \geq 0$ and 10° for $Ri < 0$. Over the sea the values are 20° and 0° for stable and unstable stratification respectively (Otto-Bleisner, et al. 1982).

2.3 Moist convective scheme

The effects of moist convection are included in the AFGL baseline model according to the cumulus parameterization scheme of Kuo (1965). In this scheme, a cloud is formed whenever the atmosphere is unstable and the vertically integrated horizontal moisture convergence exceeds a certain threshold value.

Recently, Soong et al. (1985) added several improvements to the Kuo scheme in support of the global modelling research at AFGL. These improvements include the prediction of the height of the cloud tops and the incorporation of the effects of entrainment on the cloud temperature and specific humidity profiles. For our study, we have adapted this modified cumulus parameterization scheme.

2.4 Diagnostic cloud scheme

In the present version of the model there is no radiative transfer routine so that the main purpose of the cloud scheme is to serve as a convenient way of representing the humidity field at any particular forecast time. Thus we are concerned only with specifying cloud cover but not the radiative properties of the clouds. We are also not concerned here with the complex problem of cloud-radiation interaction. For this work we use the cloud scheme devised by Geleyn et al. (1982) in which the cloud amount, C , in any model layer is determined as a function of the relative humidity and is given by

$$C = (\max \left(\frac{RH - RH_c}{1 - RH_c}, 0.0 \right))^2 \quad (14)$$

where RH is the layer relative humidity and RH_c is a critical value which is a function of the vertical coordinate given by

$$RH_c = 1 - 2\sigma(1-\sigma)[1 + \sqrt{3}(\sigma - \frac{1}{2})] \quad (15).$$

The total cloud cover in a column is specified by maximum overlap, i.e. the total is set equal to the maximum layer value in the column.

3. EXPERIMENTS AND RESULTS

In this section we describe the experiments that we conducted and their results. In view of our limited computer resources we found it necessary to choose between the number of experiments and the spatial resolution of the model. In order to obtain meaningful statistics for the significance of our results, it was preferable to run as many test forecasts as possible. Thus for most of our work we used a resolution of nine equal thickness sigma layers in the vertical and rhomboidal 15 truncation in the horizontal. The corresponding transform grid is 40 latitude by 48 longitude points ($4.4^\circ \times 7.5^\circ$). This is comparable to the resolution used in many spectral climate models (e.g. Pitcher et al., 1983). We will refer to these cases as low resolution and designate them as 15R9. All of the experiments presented below were run on either a Digital VAX 11/750 or a Microvax 11. With a time step of 45 min, the 15R9 model requires 62 min of CPU time per forecast day. In one particular case, we increased the horizontal resolution to rhomboidal 23 corresponding to a transform grid of 60 latitudes by 72 longitudes ($3^\circ \times 5^\circ$). This will be designated 23R9.

3.1 Data sources

For the experiments presented below, we obtained data from the European Center for Medium Range Weather Forecasts (ECMWF). An extensive archive of daily global analyses (00Z and 12Z) beginning from 1980 is maintained at ECMWF. These data sets consist of initialized values of wind components, geopotential height, temperature,

relative humidity, and vertical velocity. The data are available on a $2.5^\circ \times 2.5^\circ$ grid at the following seven mandatory pressure levels: 1000, 850, 700, 500, 300, 200, and 100 mb.

The data can be requested in a choice of tape formats. We originally ordered a tape written in a compressed binary mode in which up to three months of data (either 00Z or 12Z) can be stored on a single nine track tape at 1600 bpi. After several frustrating and unsuccessful attempts to read this tape we reordered the data in the WMO-GRID format which is a compressed code written in ASCII characters. In this format, up to 23 days of data can be stored on a single tape. Reading the tape was fairly straightforward, but it took us several weeks to write the appropriate software to remove extraneous control characters and to decode the data. In the end, we obtained the 12Z data for the forty five day period from 17 October through 30 November 1986. We chose this period since it included several storms which crossed the Mediterranean and brought significant rain to Israel and the surrounding area.

3.2 Low resolution experiments

In this section we present the results of a series of low resolution (15R9) experiments in which we examined the sensitivity of the model produced precipitation to changes in the sea surface temperatures of the eastern Mediterranean. We ran a series of eleven 96 hour forecasts covering successive four day periods beginning from 12Z on 17 October 1986. Thus, the initial data for the eleven forecasts consisted of the 12Z analyses on 17, 21, 25, 29 October, 2, 6, 10, 14, 18, 22, and 26 November 1986. From each of these initial times, we ran two forecasts. In the control forecast

(designated CONT) we used climatological monthly mean sea surface temperatures. In the anomaly forecast (designated ANOM) we increased the sea surface temperature of the eastern Mediterranean by 2°C in the Ionian Sea and by 2.5°C in the Levantine Sea. The value of 2.5°C is four times the standard deviation of the multiyear observed winter surface temperature of the eastern Levantine Sea (Hecht et al., 1988). Thus in our experiments, this anomaly is meant to represent an upper limit on the range of the interannual variability of the eastern Mediterranean (i.e. ± 2 standard deviations). We chose a forecast period of 96 hours for two reasons. First, this is close to the skillful forecast limit of this particular model configuration (i.e. low resolution with no radiative transfer routine). Second, we felt that this was a long enough period to allow for the spin up of the divergence and moisture fields in the model.

Our main interest in this study is the sensitivity of the model produced precipitation to changes in sea surface temperatures. Thus we will only briefly address the issue of performance and verification in order to demonstrate the capabilities of the model. To this end, in Figure 1 we show the global root mean square (RMS) 1000-200 mb height error for the eleven control forecasts. If we use persistence as a measure of the performance limit, then at four days the model still shows some skill. Extrapolation of these two curves indicates that the model will no longer be skillful (i.e. it would lose to persistence) at about 4.5 days. With this as background, we now proceed to the main results of this study, i.e. the precipitation and cloud forecasts. We again emphasize that our interest is the sensitivity of the model and so we will focus our discussion on the model results and not on verification against observed values.

Figure 2 shows the twelve day (three forecasts) running mean rainfall in mm day⁻¹ for the region bounded by

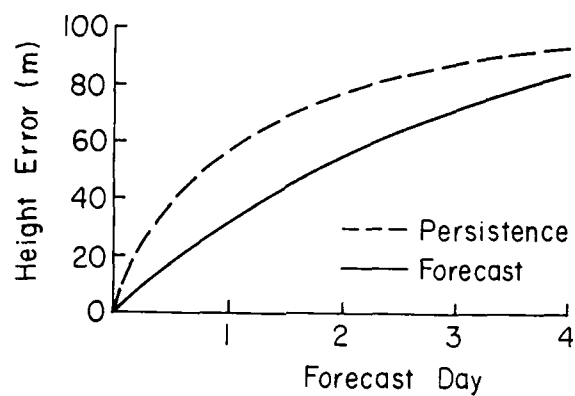


Figure 1: Root mean square (RMS) height error for the layer 1000-200 mb for the eleven control forecasts with the 15R9 model.

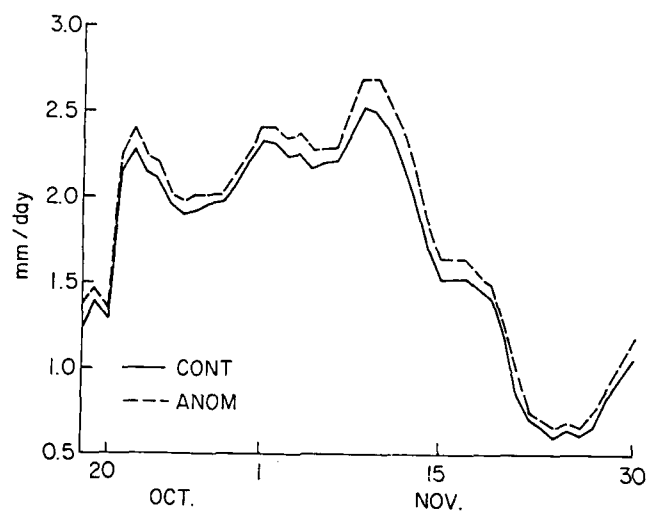


Figure 2: Twelve day running mean rainfall in mm day⁻¹ over the region 20°-50°N, 20°-45°E. Solid line - control forecasts; dashed line - anomaly forecasts.

20°-50°N, 20°-45°E. For each of the forty four forecast days, the anomaly rainfall exceeds the corresponding control amount. The pronounced peaks on 22 October, 2 November, and 8 November correspond to three major storms that passed through the region. From 9-24 November there were no storms as indicated by the sharp decrease in the mean rainfall during that period. The trend reverses on 26 November when another storm appeared in the region. The largest differences between the control and anomaly amounts tend to be at the times of the most intense rainfall (i.e. at the peaks in the curves).

In Figure 3 we show the total rainfall in mm day⁻¹ for the entire forty four days of the eleven control forecasts. There are three regions where the precipitation field exhibits relative maxima. The most intense is located in the northwest corner of the map off the Atlantic coast of France. This is associated with North Atlantic storms which cross central and northern Europe. In general, these storms do not affect the eastern Mediterranean region. The second maximum appears as a tongue of precipitation greater than 3 mm day⁻¹ over the Adriatic Sea and Yugoslavia. The third maximum occurs over the eastern end of the Mediterranean (values greater than 2 mm day⁻¹) and extends eastward into Iraq (off the edge of the map). The regions of minimum rainfall include North Africa and the part of the Soviet Union just north of the Black Sea as indicated by the closed 1 mm day⁻¹ contour.

The changes in the precipitation field for the entire forty four day period is shown in Figure 4 where we have plotted the values of ANOM-CONT. The shading indicates statistical significance at or above the 90% level based on a t-test for paired comparisons. The significant increase in precipitation is confined mainly to the Levantine Sea and the surrounding area. Maximum values of 0.6 mm day⁻¹ or more appear as a band which follows the coast of Turkey. Over

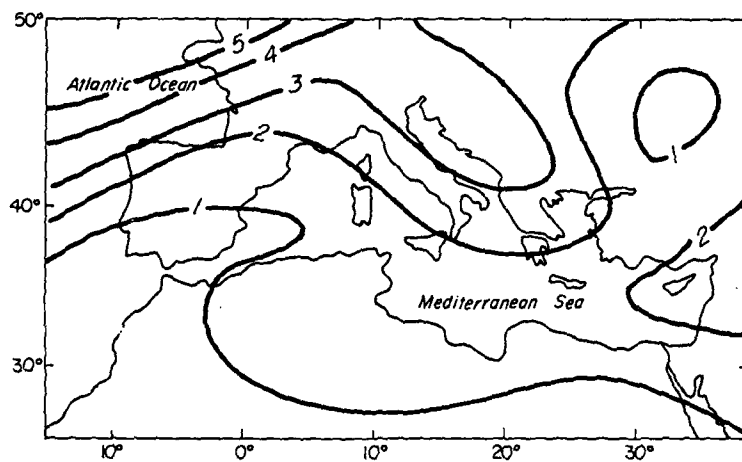


Figure 3: Total rainfall in mm day^{-1} for the entire forty four day period of the eleven control forecasts. The contour interval is 1 mm day^{-1} .

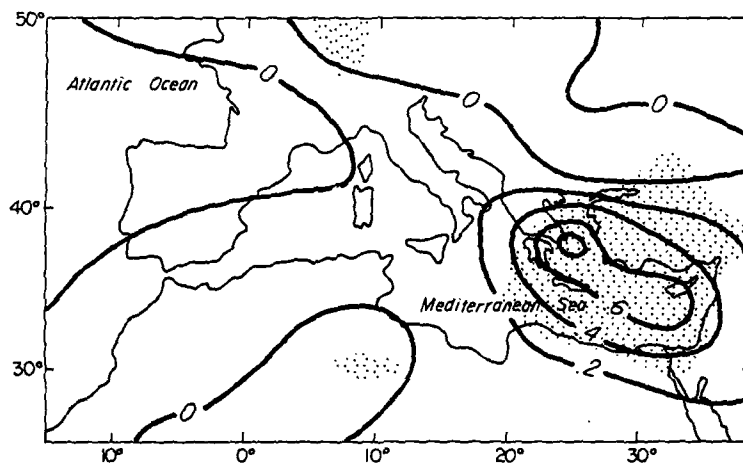


Figure 4: ANOM-CONT rainfall difference for the same period as in Figure 3. Shading indicates statistical significance at or above the 90% level. The contour interval is 0.2 mm day^{-1} .

central and northern Israel and Lebanon, the increase of 0.4 mm day^{-1} corresponds to 15-20% of the total rainfall for that area. There is a slight decrease in the rainfall across eastern Europe, over Algeria, and over parts of Spain and France. However these decreases are not significant except for the two very small areas indicated on the map.

The obvious source of moisture for storms that enter into or develop over the Mediterranean region must be the sea. The role of the Mediterranean as a source of evaporation is further enhanced by its nature of being a warm semi-enclosed sea. This effect is analogous to the role of the Great Lakes in enhancing winter snowfall over the so called "snow belt" as cold storms from Canada cross over the relatively warm lakes. In Figure 5 we show the total latent heat flux from the sea (expressed as evaporation in mm day^{-1}) for the eleven control forecasts. The eastern Mediterranean with its relatively high surface temperatures stands out with a maximum of over 6 mm day^{-1} to the south of Cyprus. The western Mediterranean appears to be of much less importance. The values for evaporation are reasonable compared to those computed by Bunker (1972) based on ship observations. The values of the model sensible heat flux from the sea (not shown here) are typically less than 20% of the latent heat flux. Once again this seems reasonable compared to the computations of Bunker (1972).

In Figure 6 we show the increase in evaporation for the eleven anomaly forecasts in mm day^{-1} . It is not surprising to find that the maximum increase occurs over the eastern Mediterranean. The percent increase in evaporation is comparable to the percent increase in rainfall over the region thus indicating that most of the additional moisture in the anomaly cases falls out as precipitation locally.

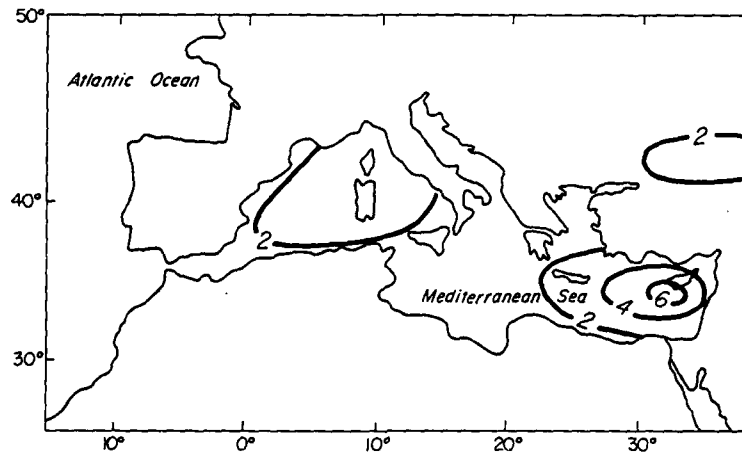


Figure 5: Total latent heat flux from the sea expressed as evaporation for the eleven control forecasts. The contour interval is 2 mm day⁻¹.

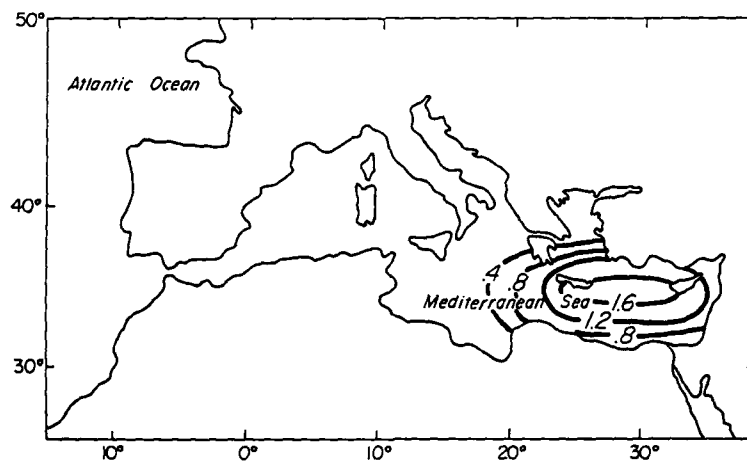


Figure 6: Increase in evaporation for the eleven anomaly forecasts (ANOM-CONT). The contour interval is 0.4 mm day⁻¹.

In order to further understand the physical processes responsible for this increase in precipitation we compared the mean circulation for the control and anomaly runs in the lowest model layer. We found that the wind components and the height field did not differ substantially (e.g. ANOM-CONT differences in the wind components were at most a few tenths of a meter per second). However, the temperature of the lowest model layer did show significant changes as indicated in Figure 7. Over the area of the imposed sea surface temperature anomaly, the mean temperature for the eleven anomaly forecasts was at least 0.5 K warmer than in the corresponding control cases. This is due to the change in the sensible heat flux from the warmer sea in the anomaly runs. The maximum sensible heat flux to the south of Cyprus increased from 44 W m^{-2} for the control runs to 67 W m^{-2} in the anomaly runs.

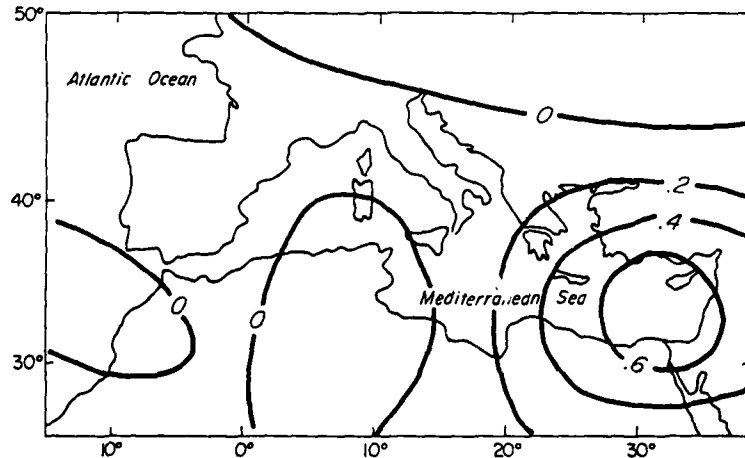


Figure 7: ANOM-CONT difference in the temperature of the lowest model layer for the entire forty four day period. The contour interval is 0.2 K.

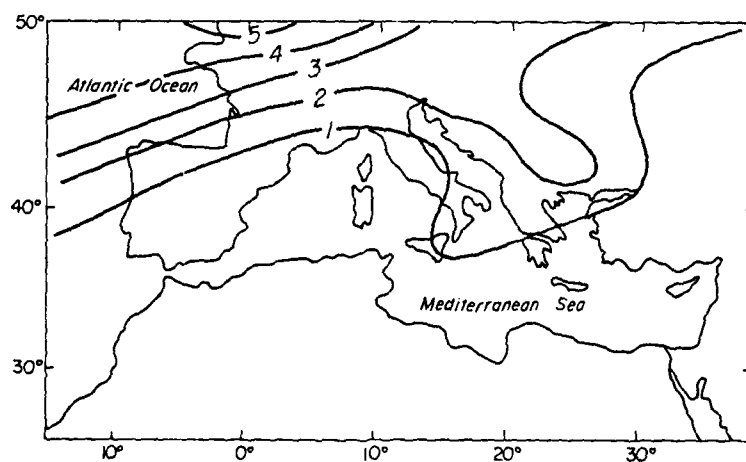


Figure 8: Large scale rainfall for the entire forty four day period of the eleven control runs. The contour interval is 1 mm day⁻¹.

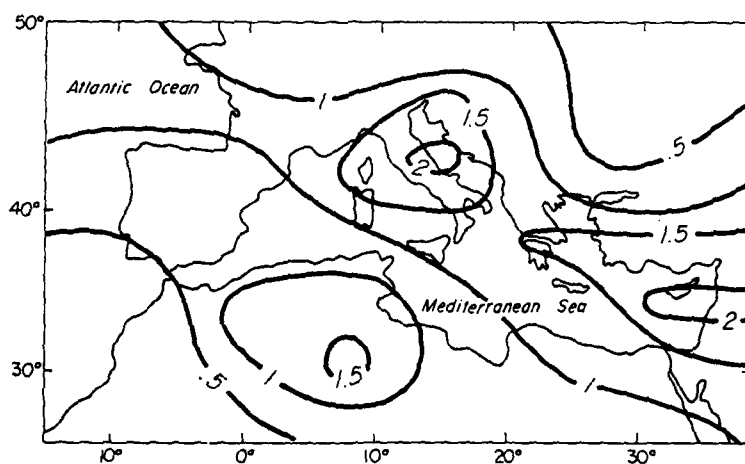


Figure 9: As in Figure 8 except for the convective rainfall. The contour interval is 0.5 mm day⁻¹.

This increase in the temperature of the lowest layer led us to suspect that perhaps the static stability decreased and as a result, the convective activity increased in the anomaly runs. We were able to check this since the model computes and saves the large scale and convective rainfall separately. Figures 8 and 9 show the large scale and the convective components, respectively, of the total control rainfall shown in Figure 3. Recalling the three precipitation maxima from Figure 3, we can now see that the maximum in the northwest corner of the map is due mainly to large scale precipitation. The land based part of the high rainfall tongue that appeared over Yugoslavia is mainly due to the large scale while the part of this tongue over the Adriatic Sea is due to convective activity. It appears that the former is related to orographic lifting while the latter is related to convective activity over the relatively warm sea. The third maximum which extended from the Levantine Sea across Israel, Lebanon, Syria and into Iraq is due almost exclusively to convective rainfall. There is also one additional maximum of convective activity over Algeria and Libya which did not stand out in the total rainfall map in Figure 3. One final point to note in Figure 9 is that the convective rainfall occurs in a band that is oriented along the major axis of the eastern Mediterranean. It seems that the convective activity is triggered by the temperature contrast between the relatively warm sea and the cold land surfaces to the north.

We conclude this section with Figures 10 and 11 which show the increase in large scale and convective rainfall, respectively, for the anomaly forecasts. These are the two components of the total change that was shown in Figure 4. It is not surprising to note that the major changes appear over the eastern Mediterranean in both components of the rainfall. This is due to the increase in available moisture by the enhanced evaporation in the anomaly forecasts. It is interesting to note that the convective rainfall contributes

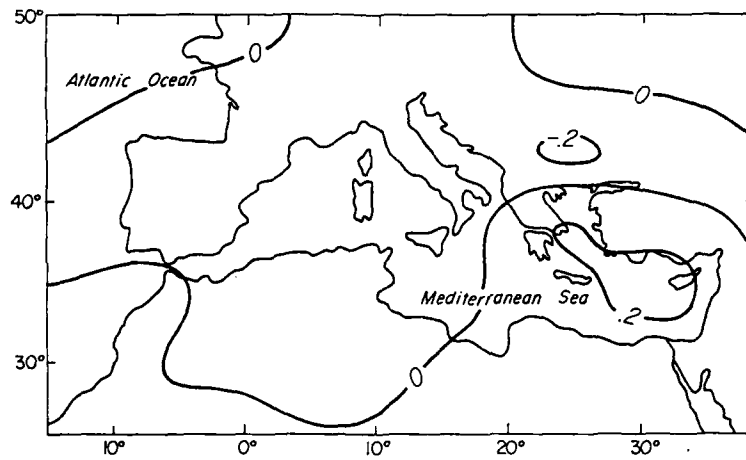


Figure 10: ANOM-CONT difference in large scale rainfall for the eleven cases. The contour interval is 0.2 mm day^{-1} .

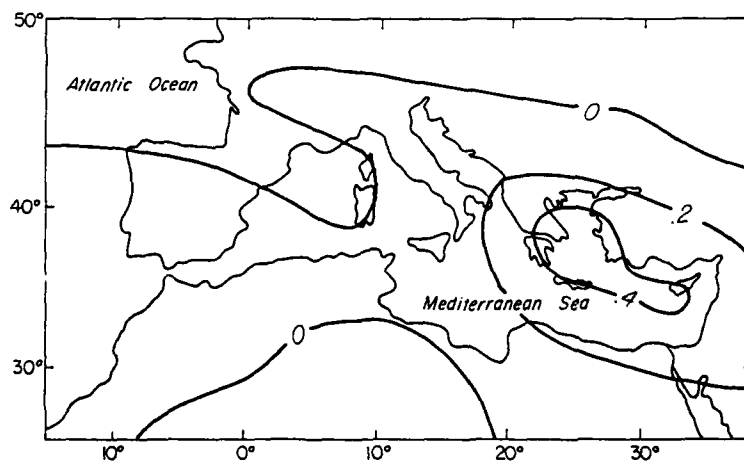


Figure 11: As in Figure 10 except for convective rainfall.

two thirds of the total increase while the large scale accounts for only one third of the total increase. Thus we can see that the increase in rainfall over this region caused by a warm sea surface temperature anomaly in the eastern Mediterranean is due to increased moisture availability through enhanced evaporation and increased convective activity triggered by heating of the atmosphere from below by an enhanced sensible heat flux.

3.3 Case study - 6 November 1986

In order to further examine the sensitivity of the model we chose one case from the eleven discussed above and ran a series of forecasts with a range of values for the sea surface temperature anomaly. For this case, we also ran several forecasts at a higher horizontal resolution (23R9)

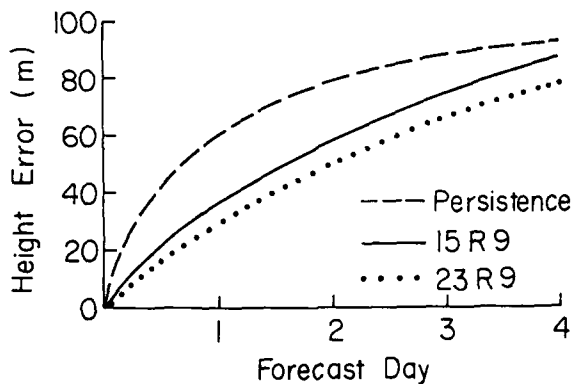


Figure 12: Global RMS 1000-200 mb height error for the control forecasts from 12Z 6 November 1986. Solid line - 15R9, dotted line - 23R9, and dashed line - persistence.

for comparison with the low resolution runs. The forecasts for this case study were run from the initial data at 12Z on 6 November 1986. This particular case was chosen since it corresponds to the highest rainfall rate in Figure 2. As in the previous section, before presenting the main results, we briefly address the performance of the model. In Figure 12 we show the global RMS 1000-200 height error for the 15R9 and 23R9 control forecasts for the 6 November case. We also include the persistence curve for comparison. As expected, the 23R9 error is smaller than the 15R9 error. Extrapolation of these curves indicates that the higher resolution forecast retains its skill for about one day longer than the lower resolution forecast.

The synoptic situation on 8 November (day of maximum predicted rainfall) is depicted in Figures 13 and 14 where we show the 48 hour 23R9 forecast 1000 mb and 500 mb height fields, respectively. This is a very typical winter rain producing situation for the eastern Mediterranean and the surrounding area. The main surface low is centered over eastern Turkey (off the edge of the map) with a cold front extending to the southwest across the Levantine Sea. There is also a hint of a secondary Cyprus low developing. Strong upper level support for this system is apparent in the 500 mb map. The trough extends across the Levantine Sea and the strong northerly winds supply this system with cold polar air which is a major ingredient necessary for heavy rain in this region.

In Figures 15 and 16 we show the total rainfall for the 15R9 and 23R9 control forecasts from 6 November. The general pattern is similar for both forecasts although there are certainly some noticeable differences in the details. Both resolutions correctly show the heaviest rainfall associated with the cold front over Turkey and the eastern Mediterranean with maximum values of over 6 mm day⁻¹. However, in the 23R9 run the sharpness of the cold front is better defined

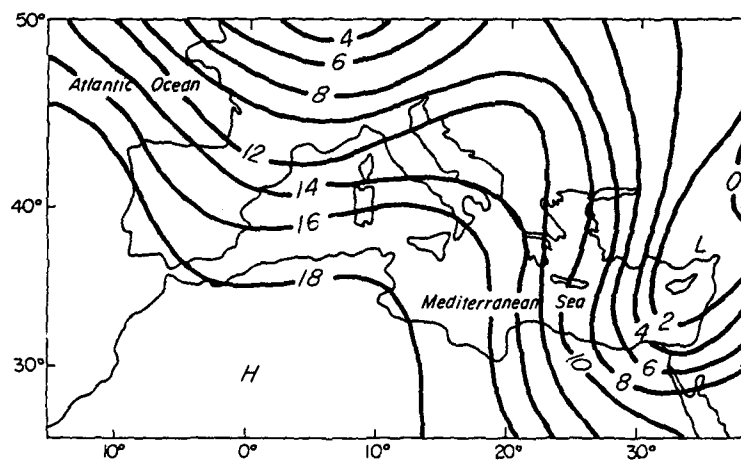


Figure 13: 1000 mb height 48 hour CONT forecast for 8 November 1986 with the 23R9 model. The contour interval is 2 decameters.

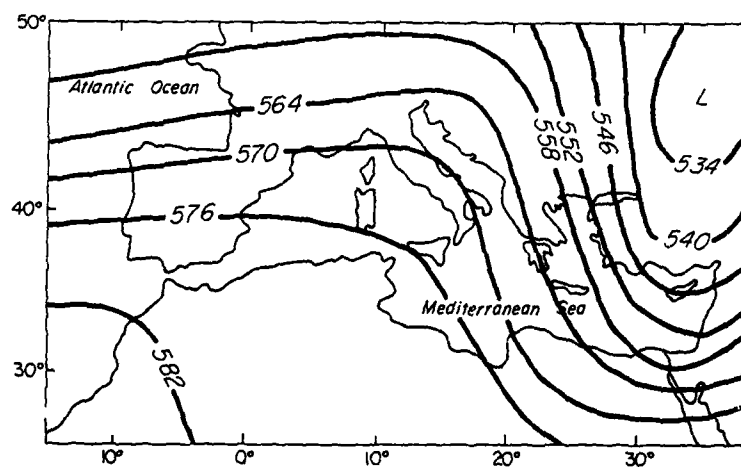


Figure 14: As in figure 13 except 500 mb heights. The contour interval is 6 decameters.

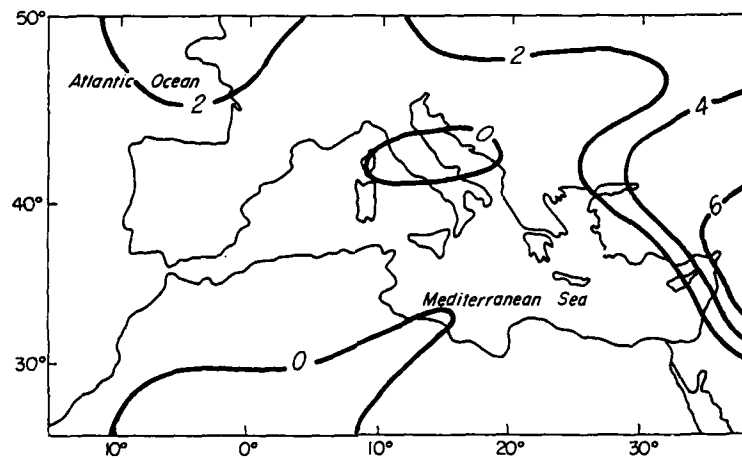


Figure 15: Total rainfall for 7-10 November for the 15R9 CONT forecast. The contour interval is 2 mm day⁻¹.

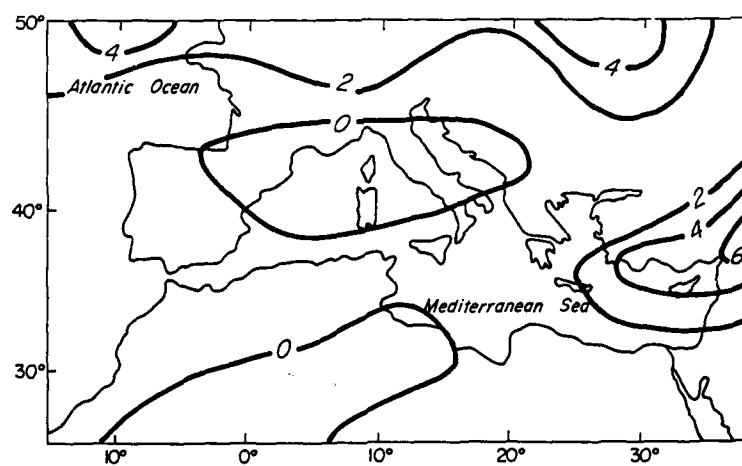


Figure 16: As in Figure 15 except for the 23R9 CONT forecast.

and the heavy rainfall ($> 4 \text{ mm day}^{-1}$) is restricted to a much narrower band around the front. The other noticeable differences are the appearance of two regions of higher rainfall along the northern edge of the map on the 23R9 forecast, and the region of no rainfall centered over Italy is much broader in the 23R9 map.

Figures 17 and 18 show the changes in rainfall for the 15R9 and 23R9 anomaly forecasts, respectively. As in the case of total rainfall, the overall patterns for the two resolutions are similar although they do differ in detail. Both exhibit an increase confined mainly to the area of the imposed sea surface temperature anomaly and extending eastward. Thus in the anomaly runs, the area of maximum rainfall is shifted southward and eastward. The maximum increase is larger by 0.4 mm day^{-1} in the 15R9 case. This difference, however, is related to the effective strength of the sea surface temperature anomaly which is somewhat weaker in the 23R9 case. Due to the difference between the size of the grid boxes in the two resolutions and the resulting difference in the area of the sea (i.e. the land sea mask), it is difficult to apply exactly the same strength anomaly to the two models. The other difference between the two figures is the region of decreased rainfall (indicated by shading). In the 15R9 case, it appears as a broad T-shaped feature while in the 23R9 case it broken up into three separate areas. Nevertheless, the patterns do resemble one another. Although it is difficult to generalize on the basis of one test case, we feel that the qualitative similarities between the low and higher resolution results are encouraging and further support the conclusions we reached in Section 3.2 which were based only on the low resolution model.

We noted above that the intensity of the sea surface temperature anomaly used in these experiments was meant to represent an upper limit on the observed range of interannual variability. The next question of course is how important is

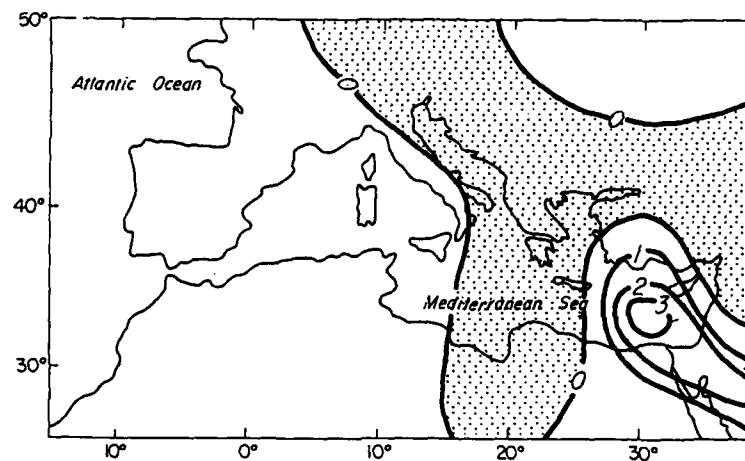


Figure 17: ANOM-CONT difference in total rainfall for 15R9 forecast from 6 November 1986. Shaded areas are negative. The contour interval is 1 mm day⁻¹.

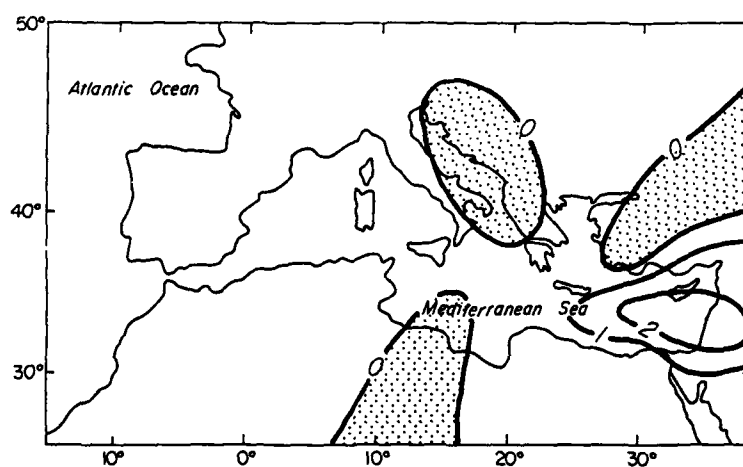


Figure 18: As in Figure 17 except for the 23R9 forecast.

the magnitude of the anomaly is changing the rainfall. To address this question we ran several additional experiments for the 6 November case in which we added sea surface temperature anomalies in the same locations but of different magnitudes. For the 15R9 model, in addition to the standard value of $+2.5^{\circ}\text{C}$ in the Levantine Sea, we also tried anomalies of -2.5°C , $+1.0^{\circ}\text{C}$, and $+4.0^{\circ}$. For the 23R9 model we also tried a value of -2.5°C . The results are shown in Figure 19

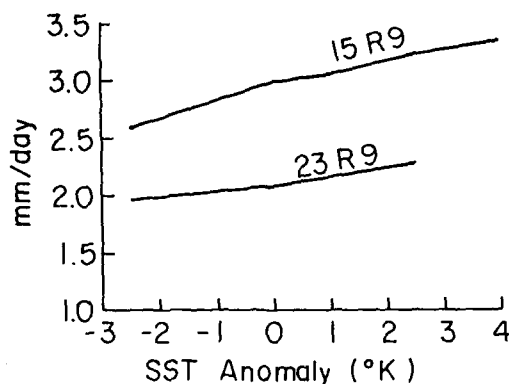


Figure 19: Total rainfall over the area 20° - 50°N , 20° - 45°E for the 6 November case as a function of the magnitude of the sea surface anomaly in the Levantine Sea.

where we show the total rainfall over the region 20° - 50°N , 20° - 45°E as a function of the magnitude of the sea surface temperature anomaly in the Levantine Sea. From these two curves we can clearly see the general trend for the rainfall to increase with the magnitude of the sea surface temperature anomaly. For the 15R9 case, the fluctuations of the area averaged rainfall are about $\pm 15\%$ of the CONT (i.e. zero anomaly) case. At the upper end of the curve, there is a hint that the rate of increase will gradually level off and possibly reach some asymptotic value. For the 23R9 runs, the fluctuations are much less dramatic. Furthermore, the consistently lower values in the 23R9 runs, as compared to

15R9, are related to the differences in resolution and the ability of the 23R9 model to better represent smaller scale variations in the humidity field. In any event, these results indicate that influence of the eastern Mediterranean on the rainfall is very localized and is confined mainly to the area over and immediately surrounding the sea.

In Figure 20 we show the change in rainfall for the -2.5°C anomaly run with the 23R9 model. As in the other cases, the maximum change (decrease in this case) occurs over the area of the imposed sea surface temperature anomaly. The magnitude of the decrease here is not as large as the corresponding increase for the $+2.5^{\circ}\text{C}$ anomaly (compare to Figure 18). We note that the cold anomaly is quite effective in suppressing most of the rainfall over southern Israel, Jordan and Saudi Arabia. For this particular case, the cold anomaly has caused the band of maximum precipitation to become narrower and shifted to the north.

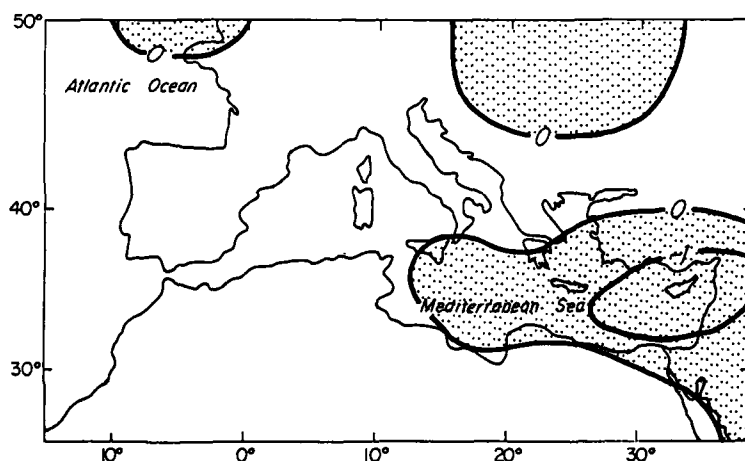


Figure 20: ANOM-CONT rainfall difference for the 23R9 cold (-2.5°C) anomaly forecast from 6 November 1986. Shaded areas are negative. The contour interval is 1 mm day^{-1} .

We conclude this section with some results of the cloud forecasts for the 23R9 model. Figure 21 shows the 48 hour control forecast for total cloud cover at 12Z on 8 November 1986. A comparison with the synoptic situation as shown in Figures 13 and 14 indicates a reasonable distribution of cloud cover. The two bands of heavy clouds - along the eastern edge and in the northwest quadrant of the map - are associated with the two lows that appear in the 1000 mb height forecast (Figure 13). The region of clear skies associated with the high over northwest Africa is also well predicted. The cloud cover for the anomaly run is very similar and is not shown here. In Figure 22, we show the cloud forecast for the cold anomaly (-2.5°C) run which differs substantially from the control forecast over the eastern Mediterranean region. The maximum cloud cover has been reduced and the band of heavy clouds has shifted to the northwest. The southern half of the Levantine Sea is now clear as compared to partly cloud or cloudy in the control forecast.

4. CONCLUSIONS

We have presented the results of a series of numerical experiments designed to study the influence of the eastern Mediterranean Sea on the precipitation in the Middle East. We concentrated our attention on the period from 17 October through 30 November 1986 which was a relatively wet period for this region.

In the first set of experiments we ran a series of consecutive 96 hour forecasts with a low resolution (15R9) modified version of the AFGL global model. In one set of runs we used climatological monthly mean sea surface temperatures while in the second set we introduced a warm sea surface temperature anomaly of 2° - 2.5°C in the eastern Mediterranean.

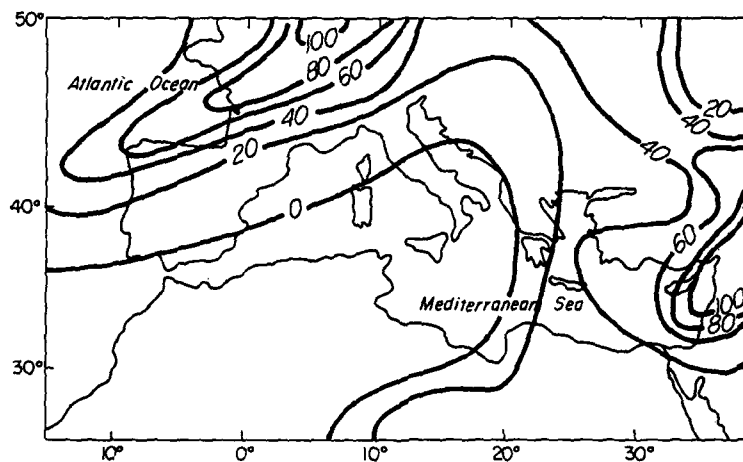


Figure 21: 48 hour control total cloud cover forecast from the 23R9 model for 8 November 1986. The contour interval is 20%.

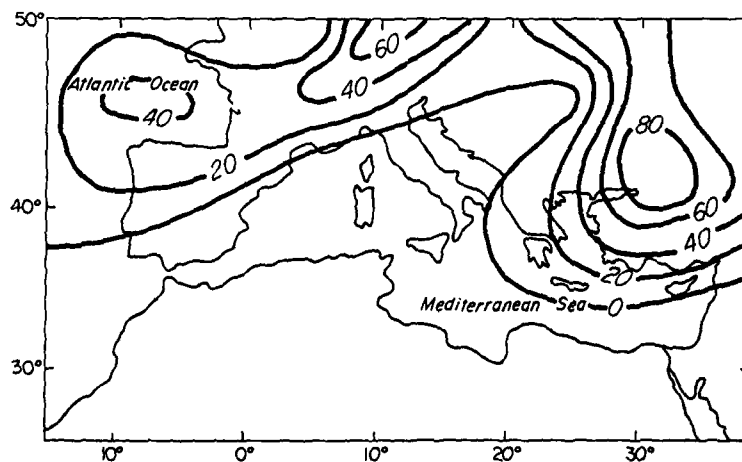


Figure 22: As in Figure 21 except for the cold anomaly forecast.

In the control forecasts, it was found that the rainfall over the eastern Mediterranean region and the Middle East was produced almost exclusively by the moist convection scheme as compared to the rainfall over western Europe which was produced by the large scale scheme. The convective rainfall occurs in a band which is oriented along the major axis of the eastern Mediterranean and is related to the temperature contrast between the relatively warm sea and the cold land surface to the north.

The introduction of a warm sea surface temperature anomaly to the eastern Mediterranean caused an increase in the rainfall over the region. The increase appeared primarily in the convective precipitation. This increase is due to the combined effects of enhanced sensible and latent heat fluxes from the warmer anomaly sea surface. The latent heat flux provides additional moisture while the sensible heat flux warms and destabilizes the lower atmosphere and leads to an increase in convective activity.

We then conducted a case study for the forecast from 6 November 1986. For this case we ran a series of experiments in which we varied the magnitude of the sea surface temperature anomaly. For the values tested, it was found that the rainfall increased monotonically with the magnitude of the anomaly. At the higher end of the range there was some indication that the rainfall may reach some asymptotic limit. We also ran several experiments in which the horizontal resolution of the model was increased. A comparison of the high and low resolution forecasts shows good qualitative agreement in the location, intensity, and pattern of the precipitation field. However there are some differences in the details which are due to the ability of the higher resolution model to better represent the smaller scale variations in the humidity field. Nevertheless, the general agreement between the low and high resolution runs is quite encouraging.

5. REFERENCES

- Arakawa, A. and V.R. Lamb, 1977: Computational design of the basic dynamical processes of the UCLA general circulation model. Methods in Computational Physics, Vol 17, Academic Press, New York, 174-265.
- Bunker, A.F., 1972: Wintertime interaction of the atmosphere with the Mediterranean Sea. J. Phys. Oceanogr., 2, 225-238.
- Bourke, W., B. McAveney, K. Puri, and R. Thurling, 1977: Spectral methods in atmospheric modelling. Methods in Computational Physics, Vol. 17, Academic Press, New York.
- Brenner, S., 1987: Derivation of consistent surface fixed fields for use in a global NWP model. AFOSR Sci. Rep. AFOSR-87-0066-001, 19pp. GL-TR-89-0112
- , 1988: A comparison of various numerical solutions of the hydrostatic equation. Reprints of the Eighth Conference on Numerical Weather Prediction, 22-26 February 1988, Baltimore, MD. American Meteorological Society, 438-441.
- , S., C.H. Yang and S. Yee, 1982: The AFGL spectral model of the moist global atmosphere: Documentation of the baseline version. AFGL Tech. Rep. 82-0393, 65 pp. ADA129283
- , C.H. Yang and K. Mitchell, 1984: The AFGL global spectral model: Expanded resolution baseline version. AFGL Tech. Rep. 84-0308, 72 pp. ADA160370
- Cressman, G.P., 1959: An operational objective analysis system. Mon. Wea. Rev., 87, 367-374.
- Deardorff, J.W., 1968: Dependence of air sea transfer coefficients on bulk stability. J. Geophys. Res., 73, 2549-2558.
- Geleyn, J.F., A. Hense and H.J. Preuss, 1982: A comparison of model generated radiation fields with satellite measurements. Beitr. Atmos. Phys., 55, 253-286.
- Gordon, C.T. and W.F. Stern, 1982: A description of the GFDL global spectral model. Mon. Wea. Rev., 110, 625-644.
- Geernaert, G.L., K.B. Katsoros, and K. Richter, 1986: Variation of the drag coefficient and its dependence on sea state. J. Geophys. Res., 91, 7667-7679.
- Hansen, J., G. Russell, D. Rind, P. Stone, A. Lacis, S. Lebedeff, R. Ruedy, and L. Travis, 1983: Efficient three dimensional global models for climate studies. Models I and II. Mon. Wea. Rev., 111, 609-662.

Hecht, A., N. Pinardi, and A.R. Robinson, 1988: Currents, water masses, eddies, and jets in the eastern Mediterranean Levantine Basin. J. Phys. Oceanogr., 18, in press.

Kuo, H.L., 1965: On the formation and intensification of tropical cyclones through latent heat release by cumulus convection. J. Atmos. Sci., 22, 40-63.

Mahrt, L., 1987: Grid averaged surface fluxes. Mon. Wea. Rev., 115, 1550-1560.

-----, H. Pan, J. Paumier, and I. Troen, 1984: A boundary layer parameterization for a general circulation model. AFGL Tech. Rep. 84-0063, 179 pp. ADA144224

Mesinger, F., 1985: The sigma system problem. Reprints of the Seventh Conference on Numerical Weather Prediction, 17-20 June 1985, Montreal, P.Q., Canada. American Meteorological Society, 340-347.

Otto-Bleisner, B.L., G.W. Branstator, and D.D. Houghton, 1982: A global low order spectral general circulation model. Part I: formulation and seasonal climatology. J. Atmos. Sci., 39, 929-948.

Ozsoy, E., 1981: On the atmospheric factors affecting the Levantine Sea. ECMWF Tech. Rep. 25, 29 pp.

Pitcher, E.J., R.C. Malone, V. Ramanathan, M.L. Blackmon, K. Puri, and W. Bourke, 1983: January and July simulations with a spectral general circulation model. J. Atmos. Sci., 40, 580-604.

Sela, J.G., 1980: Spectral modeling at the National Meteorological Center. Mon. Wea. Rev., 108, 1279-1292.

Soong, S.T., Y. Ogura, and W.S. Kau, 1985: A study of cumulus parameterization in a global circulation model. AFGL Tech. Rep. 85-0160, 113 pp. ADA170137

Tzvetkov, E., 1985: Heat storage in the eastern Mediterranean and winter precipitation in Israel. Isr. J. Earth Sci., 34, 102-109.

-----, and G. Assaf, 1982: The Mediterranean heat storage and Israeli precipitation. Water Resour. Res., 18, 1036-1040.

Wallace, J.M., S. Tibaldi, and A.J. Simmons, 1983: Reduction of systematic forecast errors in the ECMWF model through the introduction of an envelope orography. Quart. J. Roy. Met. Soc., 109, 683-717.